JCTC Journal of Chemical Theory and Computation

Article

pubs.acs.org/JCTC

Benchmarking the *GW* Approximation and Bethe–Salpeter Equation for Groups IB and IIB Atoms and Monoxides

Linda Hung,*[,†] Fabien Bruneval,*[,§] Kopinjol Baishya,[‡] and Serdar Öğüt*[,‡]

[†]NIST Center for Neutron Research, National Institute of Standard and Technology, Gaithersburg, Maryland 20899, United States

[‡]Department of Physics, University of Illinois at Chicago, Chicago, Illinois 60607, United States

[§]CEA, DEN, Service de Recherches de Métallurgie Physique, Université Paris-Saclay, F-91191 Gif-sur-Yvette, France

Supporting Information

ABSTRACT: Energies from the *GW* approximation and the Bethe–Salpeter equation (BSE) are benchmarked against the excitation energies of transition-metal (Cu, Zn, Ag, and Cd) single atoms and monoxide anions. We demonstrate that best estimates of *GW* quasiparticle energies at the complete basis set limit should be obtained via extrapolation or closure relations, while numerically converged *GW*-BSE eigenvalues can be obtained on a finite basis set. Calculations using real-space wave functions and pseudopotentials are shown to give best-estimate *GW* energies that agree (up to the extrapolation error) with calculations using all-electron Gaussian basis sets. We benchmark the effects of a vertex approximation (Γ_{LDA}) and the mean-field starting point in *GW* and the BSE, performing computations using a real-space, transition-space basis and scalar-relativistic pseudopotentials. While no variant of *GW* improves on perturbative G_0W_0 at predicting ionization energies, $G_0W_0\Gamma_{LDA}$-BSE computations give excellent agreement with experimental absorption spectra as long as off-diagonal self-energy terms are included. We also present G_0W_0 quasiparticle energies for the CuO^-, ZnO^-, AgO^-, and CdO^- anions, in comparison to available anion photoelectron spectra.

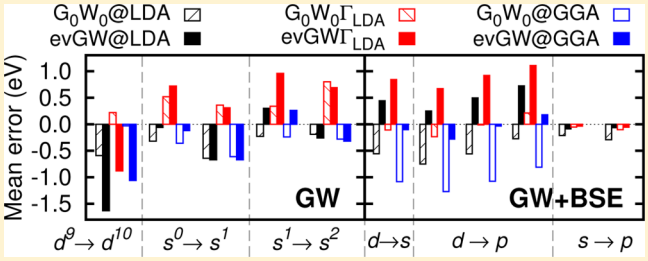

1. INTRODUCTION

Excited-state properties of transition metals are of interest for a variety of energy and electronics applications. However, quantitative simulations of one- and two-particle excitations can be difficult for these systems due to their enhanced correlation interactions. Density functional theory (DFT) calculations using hybrid exchange–correlation functionals or a Hubbard *U* interaction have been successful and computationally efficient in simulating excited-state properties of certain transition-metal systems;[1−7] however, the transferability of such functionals across a variety of materials is still being tested and verified. At the other extreme, the accuracy of quantum chemistry methods can be systematically increased, but the computational cost of post-Hartree–Fock methods is much larger.

With computational costs between that of DFT and quantum chemistry calculations, the *GW* approximation and the Bethe–Salpeter equation (BSE) provide an alternate first-principles route to modeling one- and two-particle excitations.[8−11] When the *GW* equations are solved self-consistently, the sole deviation of *GW* and *GW*-BSE from the exact one- and two-particle solutions, respectively, is the vertex approximation. Complications in interpreting *GW* and BSE results arise, however, as additional numerical and physical approximations—such as the use of finite basis sets, the pseudopotential approximation, and non-self-consistency—are applied to reduce computation time. For transition-metal systems, the impact of these approximations may be magnified due to the larger correlation energies that must be computed within the *GW* approximation. For example, *GW* calculations for the bulk ZnO band gap received particular attention after values were published in a wide range from 2.1 to 3.9 eV, as discussed in ref 12 and references therein. Materials containing transition-metal atoms thus act as a rigorous test set for many-body perturbation theory, and earlier benchmarks examining the effects of core–valence electron partitioning, mean-field starting points, self-consistency, and relativistic effects have already highlighted some of the successes and obstacles in simulating such systems.[13−17]

Motivated by increasing use of the *GW* approximation and the BSE in studying excited-state properties, we benchmark the impact of various numerical and theoretical approximations on excitations of Groups IB and IIB atoms and monoxides. *GW* quasiparticle energies are computed for ground-state atoms in three valence electron configurations: d^{10} (Cu^+, Ag^+, Zn^{2+}, and Cd^{2+}), $d^{10}s^1$ (Cu^0, Ag^0, Zn^+, and Cd^+), and $d^{10}s^2$ (Cu^-, Ag^-, Zn^0, and Cd^0). For the same species, we also determine low-lying *GW*-BSE neutral excitation energies. Highly accurate reference data for the corresponding ionization and absorption energies are obtained from the NIST Atomic Spectra Database.[18] This benchmark set allows us to examine d angular momentum orbitals while avoiding complications associated with partially

Received: February 6, 2017
Published: April 7, 2017

DOI: 10.1021/acs.jctc.7b00123
J. Chem. Theory Comput. 2017, 13, 2135−2146

filled d shells, such as multiplet splitting.[19] We address the effect of the basis set and the pseudopotentials and study the influence of an approximate vertex and non-self-consistent solutions.

We begin with an overview of *GW* and BSE theory and methodologies in section 2, including discussion of the vertex approximation, eigenvalue self-consistency, and off-diagonal self-energy terms. In section 3.1, we address the basis set dependence of our computations for quasiparticles with s, p, and d character. Pseudopotential *GW* calculations on a real-space grid are compared to the Gaussian basis set, all-electron *GW* calculations for the Zn atom and cations (Zn^0, Zn^+, and Zn^{2+}), and perturbative G_0W_0 and eigenvalue self-consistent *GW* (ev*GW*) results are extrapolated to the complete basis set limit. The numerical convergence of *GW*-BSE energies relative to basis set size is presented in section 3.2. We then discuss the impact of the pseudopotential approximation, relativistic effects, and exact exchange in mean-field starting points in section 3.3. This validates the use of scalar-relativistic pseudopotentials and a real-space, transition-space implementation of *GW*-BSE within the remainder of this work and contextualizes the choice of mean-field starting points associated with local or semilocal exchange−correlation density functionals. In section 4, we benchmark the effects of the vertex approximation and non-self-consistent *GW* across our full test set. For comparison to experimental ionization energies, quasiparticle energies are obtained across six levels of *GW* theory, G_0W_0@LDA, $G_0W_0\Gamma_{LDA}$@LDA, ev*GW*@LDA, ev*GW*Γ_{LDA}@LDA, G_0W_0@GGA, and ev*GW*@GGA, where G_0W_0 is perturbative *GW*, ev*GW* is eigenvalue self-consistent *GW*, @LDA and @GGA indicate mean-field starting points of DFT with the Perdew−Wang local density approximation or the Perdew−Burke−Ernzerhof generalized-gradient approximation exchange−correlation functional, respectively,[20,21] and Γ_{LDA} is a LDA-derived two-point vertex function.[22] The *GW* quasiparticles computed at each level of theory are subsequently used in constructing and solving the BSE; the resulting eigenvalues are compared to time-dependent DFT energies and experimental absorption energies. In section 5, G_0W_0 energies for CuO^-, ZnO^-, and AgO^- are compared to experimental anion photoelectron spectra,[23−25] and the CdO^- spectrum is computed for the first time. We summarize and conclude in section 6.

2. THEORY AND METHODS

2.1. *GW* Approximation. The one-particle Green's function, whose poles are associated with energies of electron or hole injection into a system, can be expressed as the Dyson equation

$$G(1,2) = G_0(1,2) + \int \mathrm{d}(34)\, G_0(1,3)\Delta\Sigma(3,4)G(4,2) \tag{1}$$

where $(1) \equiv (\mathbf{r}_1,\sigma_1,t_1)$ is many-body notation for the spatial, spin, and time coordinates, G_0 is defined here as a mean-field Green's function (possibly including mean-field exchange and correlation effects), and $\Delta\Sigma$ is the difference between the self-energy term Σ and the mean-field exchange−correlation potential. In principle, the interacting one-particle Green's function can be determined self-consistently using four other equations that define the polarizability χ, screened Coulomb interation W, self-energy Σ, and vertex function Γ[8]

$$\chi(1,2) = -\mathrm{i}\int \mathrm{d}(34)\, G(1,3)G(4,1^+)\Gamma(3,4;2) \tag{2}$$

$$W(1,2) = V_H(1,2) + \int \mathrm{d}(34)\, V_H(1,3)\chi(3,4)W(4,2) \tag{3}$$

$$\Sigma(1,2) = \mathrm{i}\int \mathrm{d}(34)\, G(1,3)W(4,1^+)\Gamma(3,2;4) \tag{4}$$

$$\Gamma(1,2;3) = \delta(1,2)\delta(1,3) + \int \mathrm{d}(4567)\, \frac{\delta\Sigma(1,2)}{\delta G(4,5)} G(4,6)G(7,5)\Gamma(6,7;3) \tag{5}$$

where 1^+ denotes that $t_1 \rightarrow t_1 + \eta$ for some positive infinitesimal η, V_H is the bare Coulomb potential, and $\delta(1,2)$ is the Dirac delta function.

Hedin's eqs (eqs 1−5) are too computationally expensive for studying realistic systems, and instead, the *GW* approximation is typically used. In the *GW* approximation, eqs 1−4 remain unchanged, but the three-point vertex function is reduced to

$$\Gamma(1,2;3) = \delta(1,2)\delta(1,3) \tag{6}$$

which removes the need to evaluate a four-point integral. In this work, we compare the conventional *GW* approximation (with the vertex defined by eq 6) to the *GW*Γ_{LDA} method, where the two-point vertex satisfies[22,26]

$$\Gamma_{LDA}(1,2;3) = \delta(1,2)\delta(1,3) - \mathrm{i}\delta(1,2)f_{xc}(1) \times \int \mathrm{d}(45)\, G(1,4)G(5,1^+)\Gamma_{LDA}(4,5;3) \tag{7}$$

$f_{xc} = \delta V_{xc}/\delta\rho$, and V_{xc} is the LDA exchange−correlation potential.[22,27] While a three-point vertex is needed to accurately describe certain physical properties,[28−30] this two-point form of the vertex allows computations that increase the cost relative to conventional *GW* by only a prefactor (with computation time ∼30% longer than conventional *GW* in our implementation).

With our focus on atoms and molecules, we perform computations with the software suites RGWBS[26] and MOLGW,[31] both of which use a transition-space and spectral (frequency) representation of excited-state properties that is particularly efficient for evaluating *GW* and BSE energies of isolated systems. In this formulation, the conventional *GW* self-energy is partitioned into two contributions: a bare exchange part Σ^x and a correlation part Σ^c. The bare exchange self-energy matrix element between quasiparticles j and j' can be written as a sum over occupied states

$$\langle j|\Sigma^x|j'\rangle = -\sum_n^{\mathrm{occ.}} K^x_{njnj'} \tag{8}$$

where the exchange kernel is

$$K^x_{vcv'c'} = \int \mathrm{d}\mathbf{r} \int \mathrm{d}\mathbf{r}'\, \varphi_v(\mathbf{r})\varphi_c(\mathbf{r})V_H(\mathbf{r},\mathbf{r}')\varphi_{v'}(\mathbf{r}')\varphi_{c'}(\mathbf{r}') \tag{9}$$

and $\varphi(\mathbf{r})$ are real-valued quasiparticle wave functions. Because only quasiparticles j and j' and occupied states contribute to this finite summation, the evaluation of Σ^x is computationally straightforward.

This leaves the correlation term as the bottleneck for *GW* computations. In the sum-over-states formulation, the energy-dependent Σ^c is expressed as a double infinite sum over quasiparticles n and transitions s

DOI: 10.1021/acs.jctc.7b00123
J. Chem. Theory Comput. 2017, 13, 2135−2146

$$\langle j|\Sigma^{c}(E)|j'\rangle = 2\sum_{n}^{\infty}\sum_{s}^{\infty}\frac{V^{s}_{nj}V^{s}_{nj'}}{E-\varepsilon_n-\omega_s\eta_n} \tag{10}$$

where η_n is -1 for occupied state n (quasihole) and $+1$ for empty state n (quasielectron), and

$$V^{s}_{nj} = \sum_{v}^{\text{occ.}}\sum_{c}^{\text{empty}} K^{x}_{njvc}\left(\frac{\varepsilon_c-\varepsilon_v}{\omega_s}\right)^{1/2} Z^{s}_{vc} \tag{11}$$

where ε_n are quasiparticle eigenvalues (poles of G), v is the index over occupied states, and c is the index over empty states. The transition energies ω_s (poles of W) and eigenvectors with components Z^{s}_{vc} are from the solution of Casida's equations.[32] The poles of G are complex-valued, but in this framework, the quasiparticle lifetimes are assumed to be long; the imaginary part of ε_n has an infinitesimal negative value for occupied n and an infinitesimal positive value for empty n.

In addition to the exchange and correlation terms of conventional GW, $GW\Gamma_{\text{LDA}}$ has a vertex correction to the self-energy. Similar to the correlation self-energy, this vertex term also involves infinite sums. The LDA vertex contribution is

$$\langle j|\Sigma^{f}(E)|j'\rangle = \sum_{n}^{\infty}\sum_{s}^{\infty}\frac{V^{s}_{nj}F^{s}_{nj'}+F^{s}_{nj}V^{s}_{nj'}}{E-\varepsilon_n-\omega_s\eta_n} \tag{12}$$

where

$$F^{s}_{nj} = \sum_{v}^{\text{occ.}}\sum_{c}^{\text{empty}} K^{\text{LDA}}_{njvc}\left(\frac{\varepsilon_c-\varepsilon_v}{\omega_s}\right)^{1/2} Z^{s}_{vc} \tag{13}$$

and the LDA exchange–correlation kernel is

$$K^{\text{LDA}}_{vcv'c'} = \int \mathrm{d}\mathbf{r}\,\varphi_v(\mathbf{r})\varphi_c(\mathbf{r})f_{\text{xc}}(\mathbf{r})\varphi_{v'}(\mathbf{r})\varphi_{c'}(\mathbf{r}) \tag{14}$$

The vertex correction Σ^{f} is added to the bare exchange and correlation terms (eqs 8 and 10) to give the total $GW\Gamma_{\text{LDA}}$ self-energy. Note that for benchmarks simulating spin-polarized atoms or molecules in this work, the GW self-energies are evaluated separately for the spin-up and spin-down configurations, that is, spin-flip and mixed-spin interactions are not considered.

For evaluation of the correlation self-energy (eq 10) and the vertex correction (eq 12), the summations converge very slowly, especially for orbitals with larger correlation interactions. More generally phrased, the convergence with basis set size is slow. In section 3.1, we discuss how the form of the basis set and the properties of the quasiparticle under investigation affect the convergence of the GW self-energy and apply techniques to compute best estimates of energies at the complete basis set limit.

The computation of the GW self-energy is typically initialized with quasiparticles (occupations, eigenvalues, and wave functions) from a mean-field calculation. The initial electronic structure has a significant impact on "one-shot" G_0W_0 energies, although its effect can be reduced or eliminated through fully self-consistent GW iterations. Our excited-state calculations in MOLGW use DFT electronic structures computed directly within the same package, while RGWBS uses DFT electronic structures computed in PARSEC.[33]

At GW iteration k, we compute the diagonal terms of the GW Hamiltonian as

$$E^{(k)}_{jj} = E^{(k-1)}_{jj} + \text{Re}\langle j|\Delta\Sigma(E^{(k)}_{jj})|j\rangle \tag{15}$$

where $E^{(0)}_{jj}$ are the eigenvalues for the initial mean-field electronic structure and $\Delta\Sigma$ is the difference in self-energies between the current and immediately prior steps. The off-diagonal terms are computed slightly differently as

$$E^{(k)}_{ij} = \text{Re}\langle i|\Delta\Sigma(E^{(k-1)}_{ii})|j\rangle \tag{16}$$

where the energies are not renormalized to reduce computational cost. Note that because the energy dependence of Σ is not well-defined for off-diagonal terms, we choose to associate the off-diagonal self-energy with the "left" quasiparticle.

In this work, we focus on perturbative and eigenvalue self-consistent GW (or self-consistent GW in the diagonal approximation). Because wave functions remain unchanged in both types of GW calculation, contrasting G_0W_0 and evGW energies allows us to differentiate between the effects of the initial eigenvalues and the initial wave functions. Off-diagonal terms are only considered in the context of GW-BSE, in computations using smaller basis sets.

2.2. Bethe–Salpeter Equation. The energies associated with neutral excitations can be determined from the BSE, which expresses the two-particle correlation function L as[10]

$$L(1,2;1',2') = L_0(1,2;1',2') + \int \mathrm{d}(3456)\,L_0(1,4;1',3)K(3,5;4,6)L(6,2;5,2') \tag{17}$$

where

$$L_0(1,2;1',2') = G(1,2')G(2,1') \tag{18}$$

with G being a one-particle Green's function and the electron–hole interaction kernel expressed as

$$K(3,5;4,6) = -\mathrm{i}\delta(3,4)\delta(5,6)V_{\text{H}}(3,6) + \frac{\delta\Sigma(3,4)}{\delta G(6,5)} \tag{19}$$

As in the GW calculations, we use a transition-state basis in our computations. The electron–hole amplitudes of transition l can then be expressed as

$$\rho_l(\mathbf{r},\mathbf{r}') = \sum_{v}^{\text{occ.}}\sum_{c}^{\text{empty}} X^{l}_{vc}\varphi_c(\mathbf{r})\varphi_v(\mathbf{r}') + Y^{l}_{cv}\varphi_v(\mathbf{r})\varphi_c(\mathbf{r}') \tag{20}$$

for some coefficients X^{l}_{vc} and Y^{l}_{cv}. Assuming that G can be represented using quasiparticles and that electron–hole excited states are long-lived, the BSE becomes a generalized eigenvalue problem with block matrix form[34]

$$\begin{pmatrix} A & B \\ -B & -A \end{pmatrix}\begin{pmatrix} X_l \\ Y_l \end{pmatrix} = \Omega_l\begin{pmatrix} X_l \\ Y_l \end{pmatrix} \tag{21}$$

where Ω_l is the energy of an electron–hole excitation, the resonant block A corresponds to transitions from occupied to empty orbitals, and antiresonant block $-A$ corresponds to transitions from empty to occupied orbitals. The off-diagonal blocks, B and $-B$, have been found to be important for certain finite systems and are included in our calculations, that is, we do not use the Tamm–Dancoff approximation.

From the definition of the BSE kernel (eq 19), it is clear that G determines the form of A and B and significantly impacts the quality of ensuing BSE predictions. At the lowest level of approximation considered in this paper, the BSE uses G constructed directly from wave functions and energies (φ and

DOI: 10.1021/acs.jctc.7b00123
J. Chem. Theory Comput. 2017, 13, 2135–2146

ε) corresponding to the Kohn−Sham DFT electronic structure, and the BSE kernel is defined as the exchange−correlation kernel, f_{xc}. This form of the BSE is well-known as linear response time-dependent DFT (TDDFT) in Casida's formalism.[32]

In the *GW*-BSE framework, G is instead obtained from the *GW* approximation. Neglecting dynamical effects, the BSE kernel can be split into an exchange part K^x (eq 9) and a direct part

$$K^d_{vcv'c'} = K^x_{vv'cc'} + 4\sum_s \frac{V^s_{vv'}V^s_{cc'}}{\omega_s} \tag{22}$$

and the block submatrices for *GW*-BSE corresponding to the spin-conserving excitations (and ignoring spin−orbit interactions) are

$$\begin{aligned} A_{\uparrow\uparrow,\uparrow\uparrow} &= A_{\downarrow\downarrow,\downarrow\downarrow} = D + K^x + K^d \\ B_{\uparrow\uparrow,\uparrow\uparrow} &= B_{\downarrow\downarrow,\downarrow\downarrow} = K^x + K^d \\ A_{\uparrow\uparrow,\downarrow\downarrow} &= B_{\uparrow\uparrow,\downarrow\downarrow} = A_{\downarrow\downarrow,\uparrow\uparrow} = B_{\downarrow\downarrow,\uparrow\uparrow} = K^x \end{aligned} \tag{23}$$

where

$$D_{vcv'c'} = (\varepsilon_c - \varepsilon_v)\delta_{cc'}\delta_{vv'} \tag{24}$$

with c, c' being indices for empty states and v, v' being indices for occupied states, and ε_c and ε_v denote the quasiparticle energies. If the ground state is not spin polarized, its neutral excitations can be computed with a basis set two times reduced, with singlet excitations corresponding to a BSE Hamiltonian with

$$\begin{aligned} A &= D + 2K^x + K^d \\ B &= 2K^x + K^d \end{aligned} \tag{25}$$

When a vertex function is used in *GW* calculations (as in $GW\Gamma_{LDA}$), an additional vertex contribution must be added to the BSE kernel to maintain a consistent level of theory. The LDA vertex term

$$K^f_{vcv'c'} = 2\sum_s \frac{V^s_{vv'}F^s_{cc'} + F^s_{vv'}V^s_{cc'}}{\omega_s} \tag{26}$$

is added to the BSE Hamiltonian wherever K^d contributes for $GW\Gamma_{LDA}$-BSE calculations.[26] We also note that the terms V^s_{nj} and F^s_{nj} have some ambiguity in their definition during computation of the BSE kernel. Before self-consistency is reached, the old quasiparticles, which were used in calculating the *GW* quasiparticle energies, are not the same as the new quasiparticles obtained after the latest *GW* iteration; these terms can be computed with either the old or the new quasiparticles. In this work, we use V^s_{nj} and F^s_{nj} corresponding to the old quasiparticles for our perturbative *GW*-BSE calculations.

The *GW*-BSE framework outlined above most often uses G obtained from calculations using the diagonal approximation; off-diagonal terms of the *GW* self-energy are assumed to be negligible. However, past work has shown that contributions from off-diagonal terms can alter G_0W_0 and G_0W_0-BSE energies by more than 1 eV when a LDA starting point is used.[34] Off-diagonal contributions appear to be largest for unoccupied states in finite systems but can also arise for occupied states that are poorly described within DFT.[34,35] In this work, we test the impact of the diagonal approximation by performing *GW*-BSE computations that account for off-diagonal terms of the *GW* self-energy through their mean-field contribution.

In quasiparticle self-consistent *GW*, the *GW* matrix (eqs 15 and 16) is symmetrized and diagonalized to account for off-diagonal terms and generate improved quasiparticle energies and wave functions within a mean-field description.[36] However, for our comparisons to calculations in the diagonal approximation, we would like to keep the same electron density, V_{xc}, and DFT wave function basis. We compute improved quasiparticles that leave the electron density and V_{xc} unchanged by symmetrizing and then separately diagonalizing the subspace corresponding to occupied orbitals and the subspace corresponding to empty orbitals. Applying eq 24 to the transition-space basis of improved quasiparticle wave functions and then changing back to the transition-space basis of original DFT wave functions, eq 24 becomes

$$D_{vcv'c'} = \delta_{vv'}\sum_{\bar{c}} \varepsilon_{\bar{c}}\langle c|\bar{c}\rangle\langle\bar{c}|c'\rangle - \delta_{cc'}\sum_{\bar{v}} \varepsilon_{\bar{v}}\langle v|\bar{v}\rangle\langle\bar{v}|v'\rangle \tag{27}$$

where c and v are indices for the original Kohn−Sham DFT electronic structure and the overbar indicates energies and wave functions of the diagonalized quasiparticle basis. Our *GW*-BSE calculations that account for off-diagonal *GW* self-energy terms thus retain the same K^x, K^d, and K^f contributions in the BSE kernel (corresponding to the original quasiparticles), but eq 24 is replaced with eq 27.

3. NUMERICAL ACCURACY

3.1. *GW* and the Basis. In MOLGW and RGWBS, a finite set of quasiparticles and the transitions between those quasiparticles act as the basis set for computing the *GW* and BSE energies. In MOLGW, the full set of states whose wave functions can be defined on Dunning basis sets—ranging from aug-cc-pVTZ (93 basis functions) to aug-cc-pV5Z (202 basis functions)—becomes the basis for the excited-state calculations. In RGWBS, the wave functions are defined on a uniform real-space grid in a spherical domain, and calculations require convergence of the simulation cell parameters as well as the quasiparticle and transition-space basis sets. The domain must be sufficiently large and the grid sufficiently dense to accurately model the benchmarked quasiparticle wave functions' spatial extents and fluctuations.[37] These parameters are listed in the Supporting Information. In addition, for the quasiparticle and transition-space basis in RGWBS, cutoffs are used so that the quasiparticle basis set is restricted to the lowest-energy N states and the transition-space is defined by the transitions between all occupied and empty states up to state N.

As mentioned in section 2.1, the convergence of the correlation self-energy (eq 10) with basis set size is slow; therefore, the overall convergence of the *GW* self-energy is dependent on this term. Part of this basis set dependence is illustrated in Figure 1, where we plot $\mathrm{Re}\langle j|\Sigma^c(E)|j\rangle$ for j corresponding to the 3d, 4s, and 4p quasiparticles in Zn^{2+} and E is set to the DFT eigenvalue of the orbital. The correlation self-energy is partitioned into quasiparticle contributions, where each bar corresponds to the correlation self-energy associated with quasiparticles n whose energies lie within 4 eV bins (and summing over all transitions s in the basis). We observe that the 3d orbitals have correlation self-energies an order of magnitude larger than that of the 4s or 4p; this illustrates the increased difficulty in obtaining d-state correlation self-energies numerically converged to the same absolute cutoff. There are small but non-negligible contributions for both MOLGW and RGWBS from high-energy quasiparticles. We also see that the basis set choice affects the form of the high-energy quasiparticles and thus their contributions to the correlation self-energy. The atom-centered

DOI: 10.1021/acs.jctc.7b00123
J. Chem. Theory Comput. 2017, 13, 2135−2146

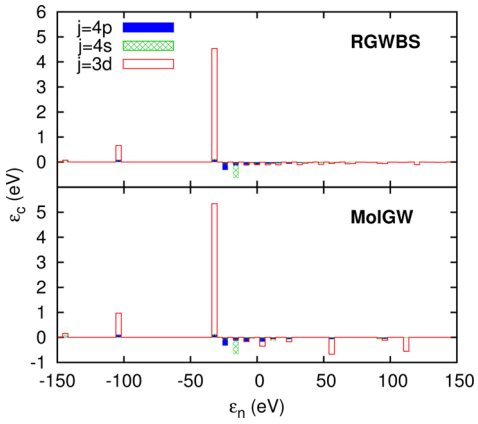

Figure 1. Contributions to the G_0W_0@GGA correlation self-energy (eq 10) for various orbitals of the Zn^{2+} ion, summed over transitions and binned every 4 eV for quasiparticle energies ε_n. These calculations truncate the correlation self-energy sum at $N = 2325$ (RGWBS) or use a aug-cc-pVTZ basis set (MOLGW). Note that MOLGW has terms in its summation outside of the range of ε_n shown here.

orbitals of MOLGW induce fewer but sharper contributions to the self-energy, compared to orbitals defined on the real-space grid of RGWBS.

The difficulties in obtaining the convergence of excited-state energies with basis set size has motivated the development and testing of techniques to obtain the complete basis set limit, including extrapolation,[38−43] the common energy denominator approximation,[44−46] construction of more efficient basis sets,[47−50] and terms to approximate the missing basis set contributions.[26,30,42,51−53] In this work, we use extrapolation to estimate the complete basis set limit after calculating G_0W_0 quasiparticle energies with a range of basis set sizes. In MOLGW, the *GW* energies at the complete basis set limit are obtained by fitting the extrapolated energy E_∞ and coefficient c_1 to

$$E(X) = E_\infty + c_1 X^{-\alpha} \tag{28}$$

where $X = 3$, 4, or 5 for aug-cc-pVTZ, aug-cc-pVQZ, or aug-cc-pV5Z, respectively. An X^{-3} dependence (equivalent to N^{-1} scaling, where N is the number of basis functions) is most commonly used for extrapolating the total correlated energy with Dunning basis sets.[54−56] However, a smaller exponent ($\alpha \approx 2$) is empirically a better fit to the quasiparticle energies computed on finite basis sets.[31,57] Later in this section, we compare extrapolated energies obtained with $\alpha = 2$ and 3.

For RGWBS, extrapolation to the complete basis set limit applies the same N^{-1} dependence suggested by earlier works, arising from the electron−electron cusp condition.[43] We fit E_∞ and coefficients c_1 and c_2 to

$$E(N) = E_\infty + \frac{c_1}{N + c_2} \tag{29}$$

The RGWBS extrapolations are performed using at least five *GW* computations at increasing values of N, and parameters E_∞, c_1, and c_2 are fit using least-squares regression weighted by N. The largest computation used to fit each extrapolation has $N > 4000$, and the DFT eigenvalue of the highest-energy state, which is a more consistent measure of convergence than the number of quasiparticles,[37] ranges from 60 to 220 eV depending on the species being studied.

Two different extrapolations are tested for RGWBS, fitting either to (1) the *GW* energy computed using the truncated correlation self-energy summation or (2) the *GW* energy from the truncated summation plus a static remainder. The remainder term in the second type of RGWBS extrapolation is derived from the static Coulomb-hole screened exchange (COHSEX) energy, which can be expressed equivalently as a sum over transitions s and as a double summation over both transitions s and quasiparticles n.[26] For a given set of transitions s, the COHSEX quasiparticle basis truncation "remainder" is the difference between the double summation evaluated up to quasiparticle cutoff N and the single summation. This COHSEX remainder can be added directly to truncated *GW* correlation energies to enhance numerical convergence.[26] However, more recently, it was shown for jellium that the high-energy contributions of the COHSEX energy overestimate the *GW* correlation terms by a factor of 2.[42,51] In this work, we therefore scale the COHSEX remainder by a factor of 1/2 to use as our static remainder.[52] An extrapolation is still used to obtain the complete basis set limit with respect to transitions s because the half COHSEX remainder acts as a closure relation only for the sum over n.

In Figure 2, the performances of MOLGW and RGWBS are compared to the experimental ionization energies of the Zn^0, Zn^+, and Zn^{2+} atoms. Each ionization energy corresponds to the energy of the quasiparticle associated with the highest occupied molecular orbital (QP-HOMO) for the same species, as well as

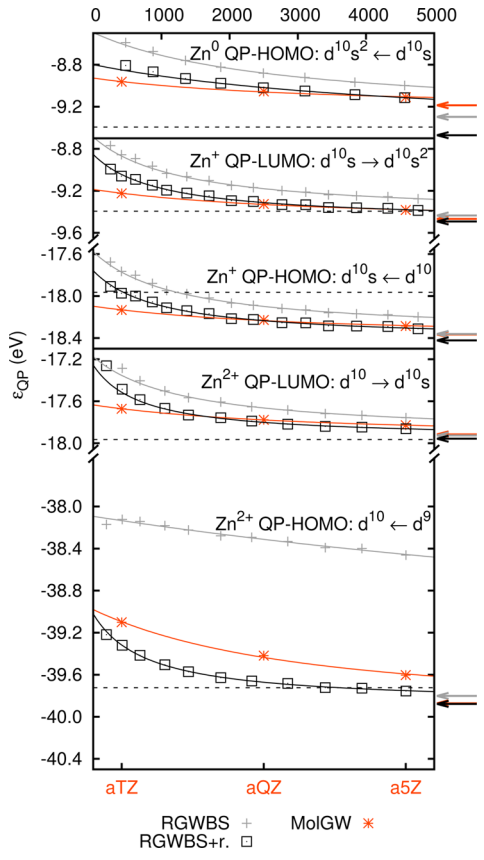

Figure 2. G_0W_0@GGA energies (eV) for Zn^0, Zn^+, and Zn^{2+} at varying basis set sizes, aug-cc-pVTZ through aug-cc-pV5Z for MOLGW (bottom axis labels) and up to more than 4000 total states for RGWBS (top axis labels). RGWBS results are shown both with and without a half COHSEX remainder term added (indicated by "+r."). Solid lines are extrapolation curves, arrows indicate the extrapolated complete basis set limits, and dashed lines indicate the negative experimentally measured ionization energies.

DOI: 10.1021/acs.jctc.7b00123
J. Chem. Theory Comput. 2017, 13, 2135−2146

Table 1. G_0W_0@GGA Energies at the Complete Basis Set Limit from All-Electron Calculations (AE) in MOLGW Using Two-Point and Three-Point Extrapolation Schemes, MOLGW Calculations Skipping the Core Electrons (AE no core), and Regular and Semicore Pseudopotential Calculations (PP) in RGWBS with and without Scalar-Relativistic Effects (rel)

	Zn^{2+}			Zn^{+}			Zn^{0}	
	3d	4s	4p	4s(↑)	4s(↓)	4p(↑)	4s	4p
AE (α = 3, 2-pt)	−39.71	−17.87	−11.91	−18.32	−9.42	−5.43	−9.14	0.80
AE (α = 2, 2-pt)	−39.87	−17.92	−11.95	−18.37	−9.47	−5.48	−9.19	0.75
AE (α = 2, 3-pt)	−40.09	−17.93	−11.99	−18.45	−9.51	−5.55	−9.27	0.62
AE no core (α = 3, 2-pt)	−38.51	−17.66	−11.80	−18.15	−9.26	−5.35	−9.01	0.83
AE no core (α = 2, 2-pt)	−38.65	−17.70	−11.84	−18.20	−9.31	−5.40	−9.06	0.78
AE no core (α = 2, 3-pt)	−38.76	−17.73	−11.86	−18.29	−9.37	−5.46	−9.14	0.66
PP (regular)	−33.67	−18.35	−12.37	−18.69	−9.75	−5.62	−9.34	0.72
PP (semicore)	−39.88	−17.96	−11.94	−18.36	−9.44	−5.45	−9.30	0.71
PP (semicore, rel.)	−39.61	−18.34	−12.07	−18.71	−9.65	−5.45	−9.69	0.80
expt	−39.72	−17.96		−17.96	−9.39		−9.39	

the quasiparticle energy of the lowest unoccupied molecular orbitals (QP-LUMO) for the species with one fewer electron. For example, the top two sets of lines in the figure both represent the $d^{10}s \rightarrow d^{10}s^2$ energy, which is the negative of the ionization energy of Zn^0; the first set of lines is the QP-HOMO energy of Zn^0 ($d^{10}s^2$ configuration) at various basis set sizes, and the second set of lines is the QP-LUMO energy of Zn^+ ($d^{10}s$ configuration). G_0W_0@GGA energies at the complete basis set limit are also listed in Table 1.

The RGWBS extrapolations shown in Figure 2 correspond to computations with a nonrelativistic semicore pseudopotential (see section 3.3). For RGWBS, the G_0W_0 energies extrapolated to the complete basis set limit are 0.1−1.4 eV lower than the most converged calculations, with the larger differences associated with quasiparticles with d character. Inclusion of the static remainder can significantly change the computed quasiparticle energies for the same basis set, but the complete basis set limit from the two RGWBS extrapolations (for self-energies computed with and without the half COHSEX term) differ by less than 0.2 eV for all Zn G_0W_0 energies. Since the two extrapolation schemes provide fairly consistent quasiparticle energies, both extrapolations are performed in the remainder of this work, and we report the extrapolated E_∞ with a smaller standard error (or better extrapolation fit). In practice, a smaller standard error for d quasiparticle energies always corresponds to the extrapolation of static-remainder-corrected sums, while either extrapolation can produce smaller error for quasiparticles with s or p character. Using extrapolations and static remainders to estimate *GW* energies at the complete basis set limit, we expect that numerical accuracy will be ∼0.1−0.2 eV, with excitations involving only s and p states having minimal numerical error from basis set effects and those with d states having numerical errors at the larger end of the range.

The MOLGW extrapolations shown in Figure 2 use a two-parameter fit and α = 2 exponent. The G_0W_0 energies at the complete basis set limit differ less than 0.1 eV from the most converged calculations, except for the 3d state, which differs nearly 0.3 eV. Thus, increased difficulty in converging d quasiparticle energies is still observed, even on a localized and atom-centered basis. Furthermore, the extrapolated d quasiparticle energy tends to have larger fluctuations depending on the choice of extrapolation scheme, as demonstrated by a comparison of the two-parameter fit with α = 2, the two-parameter fit with α = 3, and a three-parameter fit with α = 2 (where X in eq 28 is replaced with $X + c_2$). The extrapolated d quasiparticle energies vary over a range of ∼0.5 eV, while s and p quasiparticle energies are more consistent, with deviations of less than 0.2 eV (see Table 1). The largest deviations may be due to overfitting in the three-parameter extrapolation. Nevertheless, future tests across a wider benchmark set would be beneficial in quantifying the *GW* convergence properties for transition metals simulated using Dunning basis sets.

The above results show that the *GW* energies of transition-metal d states at the complete basis set limit can differ from computations on finite basis sets by more than the desired numerical accuracy of ∼0.1 eV. However, in the context of self-consistent *GW*, extrapolating energies to the complete basis set limit can quickly become prohibitively expensive for larger molecules or large basis sets. We now quantify the numerical accuracy of ev*GW* using smaller basis sets, focusing on Δ_{ev}, the energy difference between ev*GW* and G_0W_0 quasiparticles on a given basis set.

In MOLGW, the Gaussian basis functions allow efficient single-atom calculations, such that ev*GW* energies can be obtained with the same extrapolation scheme as that used for G_0W_0. The complete basis set limits of Δ_{ev}, that is, the difference between extrapolated ev*GW* and extrapolated G_0W_0 energies, are compared to Δ_{ev} computed on specific basis sets in Figure 3.

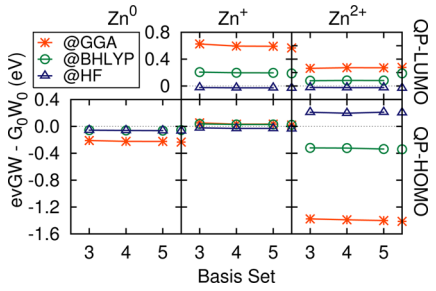

Figure 3. Difference between ev*GW* and G_0W_0 with a DFT-GGA, DFT-BHLYP (50% exact exchange), or Hartree−Fock mean-field starting point, computed in MOLGW with aug-cc-pVTZ (3), aug-cc-pVQZ (4), and aug-cc-pV5Z (5) basis sets. The points on the right border of each graph are the differences at the complete basis set limit (two-parameter extrapolation with α = 2).

The computed Δ_{ev} converge quickly with basis set size over a variety of mean-field starting points. With extrapolation exponent α = 2, the value of Δ_{ev} at the complete basis set limit differs less than 30 meV from the Δ_{ev} computed on the aug-cc-pV5Z and the aug-cc-pVQZ basis sets and also changes less than 60 meV from values computed on the aug-cc-pVTZ basis. There

DOI: 10.1021/acs.jctc.7b00123
J. Chem. Theory Comput. 2017, 13, 2135−2146

is also no noticeable difference in the convergence of Δ_{ev} associated with s, p, and d states, and the convergence of Δ_{ev} for all states is even faster with $\alpha = 3$.

We confirm that similar basis set convergence behavior occurs in RGWBS, with better convergence if the half COHSEX remainder is not used, and that the same scheme can be used for $GW\Gamma_{LDA}$ (Figure 4). In the remainder of this work, we therefore

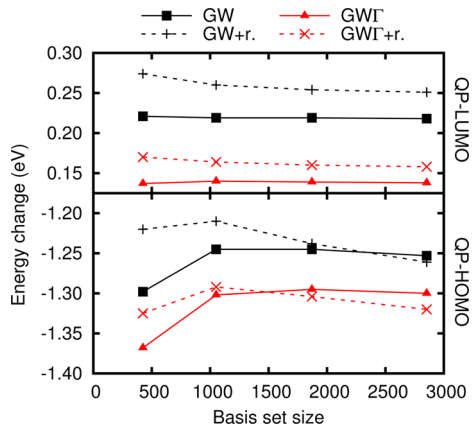

Figure 4. Difference in Zn^{2+} quasiparticle energies between evGW and G_0W_0 (with and without the LDA vertex) computed in RGWBS at various basis set sizes. Eigenvalue differences computed including the half COHSEX remainder are listed as "+r".

report the evGW energies at the complete basis set limit as $E_{\infty,evGW} = E_{\infty,G_0W_0} + \Delta_{ev}$, where E_{∞,G_0W_0} is the G_0W_0 quasiparticle energy extrapolated to the complete basis set limit and Δ_{ev} is computed from evGW and G_0W_0 calculations on smaller basis sets (~1000 states) without using the static remainder.

3.2. BSE and the Basis. Similar to GW calculations, solving the BSE requires evaluation of sums over empty states and transitions (eqs 9, 22, and 26); furthermore, the size of the BSE matrix is a function of the number of transitions. In Figure 5, we show the dependence of BSE energies on basis set size, with the three lines indicating different choices for the quasiparticle energies: (1) the energies are equal to the extrapolated best estimates regardless of the BSE basis set size, (2) the energy corresponds to a GW calculation, with the half COHSEX remainder contribution, on the same basis set as is used in the

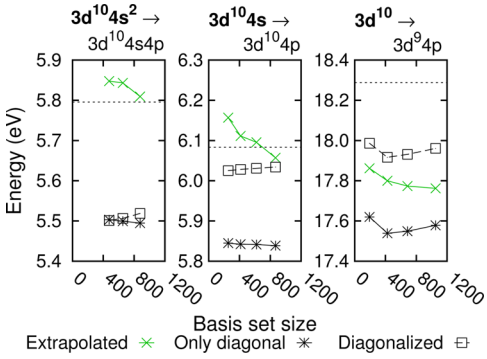

Figure 5. Convergence of the BSE computation with basis set size for the first symmetry-allowed neutral excitations of Zn^0, Zn^+, and Zn^{2+}. Experimental absorption energies are indicated by the dashed lines. See the text for descriptions 1−3 of the quasiparticle energy terms of the BSE, labeled as "Extrapolated", "Only diagonal", or "Diagonalized", respectively.

BSE calculation, and (3) the energy corresponds to a GW calculation, with the half COHSEX remainder and off-diagonal self-energy terms, on the same basis set as is used in the BSE.

For excitations between only s and p states, using the same basis set for both GW and BSE results in faster convergence of BSE eigenvalues, compared to when GW quasiparticle energies are extrapolated to the complete basis set limit. For an excitation from a d state, neither the GW-BSE results with extrapolated energies nor those with energies matching the basis set are fully converged with basis set size, but the difference is only ~0.2 eV. The inclusion of off-diagonal terms does not significantly affect convergence properties. In the remainder of this work, we therefore report results using matching basis sets for computing GW and BSE energies. With this scheme, we expect s and p excitations to be converged well within 0.1 eV, while the accuracy of the d excitations should be underestimated no more than ~0.2 eV.

3.3. Pseudopotentials, Relativistic Effects, and Hybrid Functional Mean-Field. With the finite basis set (or truncated summation) error of GW accounted for, we address a few more approximations that affect the real-space, transition-space GW-BSE calculations in section 4. This includes the use of pseudopotentials, the inclusion of scalar-relativistic effects, and the limiting of DFT mean-field starting points to LDA or GGA exchange−correlation functionals (no exact exchange in the starting point).

Table 1 lists extrapolated G_0W_0@GGA energies obtained from MOLGW and RGWBS. At the complete basis set limit, and given that MOLGW and RGWBS both use a spectral representation for GW calculations, the remaining energy differences are primarily attributed to the pseudopotential approximation. Because the accuracy of the pseudopotential approximation necessarily depends on the specific pseudopotential used, we generate high-quality multireference pseudopotentials in APE;[58,59] our Zn "semicore" pseudopotentials have radial cutoffs (r_c) of 1.3 au and $3s^23p^64s^23d^{10}$ valence (pseudized Ne core). For comparison, we also generate a "regular" Troullier−Martins pseudopotential,[60] with a pseudized Ar core and $4s^23d^{10}$ valence (r_c = 2.1 au for the s and p channels and r_c = 1.3 for the d channel). Our computations agree with past results, where the placement of the semicore states (3s and 3p for Zn) in valence, instead of pseudizing them into the core, has been shown to be essential in obtaining reasonable GW energies for d quasiparticle energies due to the spatial overlap of their wave functions.[39,61−65] The GW calculations using the regular pseudopotential result in a d quasiparticle energy for Zn^{2+} that differs more than 6 eV from the all-electron calculation, and s and p quasiparticles also exhibit significant differences up to 0.4 eV. On the other hand, the resulting quasiparticle energies from "semicore pseudopotential calculations generally lie within the range of all-electron complete basis set estimates. Differences are mostly <0.1 eV, and even the d quasiparticle differs only up to 0.2 eV from any given all-electron extrapolated G_0W_0 energy.

The pseudopotential approximation has been described as the combination of three effects: the frozen-core approximation, core−valence partitioning, and the pseudo-wave-function approximation. The frozen core approximation has little effect on overall accuracy as long as the pseudized core states and the valence electrons are sufficiently separated in energy, as is the case here when semicore electrons are treated explicitly as "valence".[66] Past work has tried to separate out solely the core−valence partitioning error associated with the pseudopotential approximation by using, as a proxy, the difference between an all-

DOI: 10.1021/acs.jctc.7b00123
J. Chem. Theory Comput. 2017, 13, 2135−2146

electron *GW* computation and the same computation with core effects removed.[66−69] However, we find it difficult to disentangle the effects of core−valence partitioning from the changes associated with pseudizing an atom's core. Our results in Table 1 instead indicate that directly ignoring the core electrons in all-electron *GW* calculations for Zn is a more drastic approximation than the pseudopotential approximation. These differences arise because of the different treatments of the nonlinearity of exchange and correlation effects. When core electrons are ignored in a formerly all-electron calculation, the computed $\Delta\Sigma$ (of eqs 1 and 15) has brute force partitioning errors from both the nonlinear *GW* energy and the nonlinear V_{xc}, which may cancel out to a certain extent. In contrast, pseudopotential generation combines the pseudization of the core potential and valence wave functions together with optimization of the partitioning (linearization) of the core and valence parts of V_{xc}, such that the eigenvalues of the Kohn−Sham orbitals match the reference all-electron eigenvalues.

We next compare scalar-relativistic and the nonrelativistic pseudopotentials. Table 1 shows that relativistic effects decrease the s and p quasiparticle energies up to 0.4 eV, while the Zn^{2+} d quasiparticle energy increases by 0.3 eV. Due to the observed importance of relativistic effects, scalar-relativistic pseudopotentials are used for all results presented in sections 4 and 5. As in the Zn pseudopotentials tested here, the cores of Cu, Ag, and Cd pseudopotentials are pseudized through multireference fits, with all semicore electrons considered part of the "valence". We also note that, for the elements studied in this work (up through period five), the use of scalar-relativistic instead of fully relativistic *GW* calculations should affect the starting point by less than 0.1 eV.[17]

Finally, we use MOLGW to study the effect of exact exchange in the mean-field starting point, performing computations where none, half, or all of the exchange density functional is replaced with a corresponding amount of exact exchange. We find that the amount of exact exchange has a significant effect at the DFT, G_0W_0, and ev*GW* levels of theory (Figure 6). As expected, the DFT LUMO become less bound while the DFT HOMO is more bound with increasing amounts of exact exchange. However, the *GW* approximation decreases or even reverses the trend observed at the DFT level, with the change in trends most evident at the ev*GW* level of theory. We therefore emphasize that optimization of only eigenvalues (ev*GW*) cannot remove the starting point dependence for this transition-metal atom, in contrast with earlier work benchmarking small water clusters.[70] In fact, the largest *GW* quasiparticle energy difference of 1.4 eV is between the QP-HOMO energies computed using ev*GW*@GGA and ev*GW*@HF, which is larger than the starting point dependence at the G_0W_0 level of theory. Combined, these trends demonstrate the importance of the quasiparticle wave functions in computing *GW* energies.

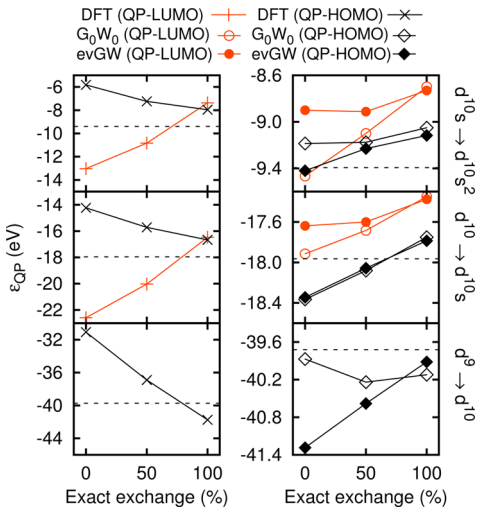

Figure 6. DFT (left), G_0W_0, and ev*GW* (right) quasiparticle energies computed with MOLGW, with mean-field starting points of 0% exact exchange (GGA), 50% exact exchange, and 100% exact exchange (HF). DFT energies are computed on the aug-cc-pV5Z basis set, and *GW* energies are at the complete basis set limit ($\alpha = 2$). Dashed lines indicate the negative experimentally measured ionization energies.

Because relativistic effects are not included in these specific all-electron calculations, we do not attempt to determine the optimal amount of exact exchange that will allow G_0W_0 or ev*GW* to match experimental ionization energies. Nevertheless, as relativistic effects are generally observed to decrease the s and p eigenvalues while increasing the value of d eigenvalues, DFT with exact exchange between 50 and 100% appears to produce the best mean-field wave functions for both the G_0W_0 and ev*GW* quasiparticle energies for the Zn atom and ions. Between 50 and 100% exact exchange, we also observe that G_0W_0 and ev*GW* energies are closest to each other in value, consistent with earlier benchmarks on an organic molecule test set, where a DFT starting point with 75% exact exchange was found to produce G_0W_0 and ev*GW* eigenvalues in the best agreement with each other, as well as with quasiparticle self-consistent *GW*.[56] A possible problem remains where the QP-HOMO and QP-LUMO that describe the same one-particle excitation do not have the same energies at any amount of exact exchange. This problem may, in part, be alleviated through the inclusion of the off-diagonal terms of the *GW* energy, which lowers the QP-LUMO.[34] However, there may be remaining differences due to the two-point vertex approximation, as mentioned earlier in section 2.1. While additional benchmarks are needed, these tests suggest that a good (system-dependent) starting point may allow excited-state energy predictions at a lower computational cost than fully self-consistent *GW* calculations, although self-consistency remains the only way to satisfy conservation laws and completely remove the starting point dependence.[71]

For the semilocal (and local) density functionals used to compute the wave functions in the remainder of this work, we expect lower accuracies for *GW* computations than if using an optimal hybrid starting point. These calculations also suggest that our benchmarked *GW* quasiparticle energies will be lower than those computed using hybrid functional wave functions, with a possible exception for G_0W_0 quasiparticles with d character.

4. VERTEX AND SELF-CONSISTENCY

4.1. Ionization Energies. We now benchmark the effects of self-consistency and the vertex function on *GW* quasiparticle energies. The accuracies of computed isovalent Cu, Ag, Zn, and Cd quasiparticle energies are compared to experiment in Figure 7. The performance of *GW* is similar across each valence electron configuration, and the mean errors are listed in Table 2.

As in past work, eigenvalue self-consistency widens the fundamental gap. The energies for QP-HOMO with s character ($d^{10}s$ and $d^{10}s^2$ valence) remain fairly similar, the energies of the QP-LUMO (all of which have s character) increase, and energies of QP-HOMO with d character (d^{10} valence) decrease. The resulting d quasiparticle energies from ev*GW* are less acccurate

DOI: 10.1021/acs.jctc.7b00123
J. Chem. Theory Comput. 2017, 13, 2135−2146

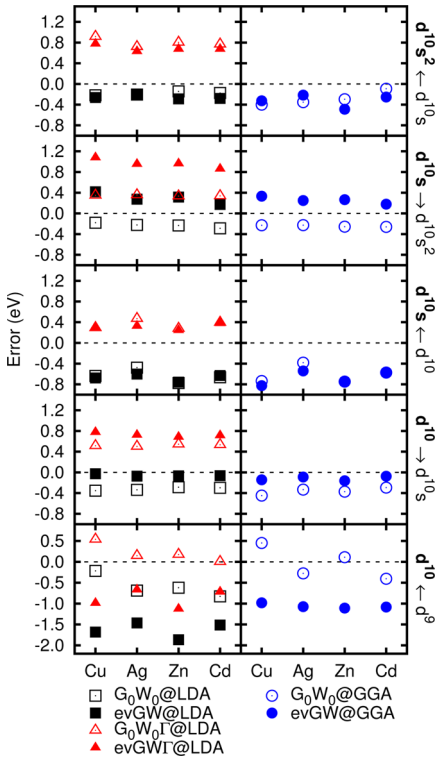

Figure 7. Error of *GW* quasiparticle energies relative to experiment, with reference valence electron configurations in bold.

than those in G_0W_0, and there is no systematic improvement for s or p states. The worsened quasiparticle energies differ from the majority of ev*GW* benchmarks of primarily sp-bonded molecules,[56,70,72,73] but similar results were observed in earlier studies of azabenzenes and small transition-metal molecules.[14,74]

In past works, the LDA-vertex-corrected *GW* has always been associated with a nearly rigid shift of all energies from conventional *GW* values.[22,30,75] Here, in contrast, the energy change associated with the vertex correction ranges from less than 0.6 eV to more than 1.1 eV. The variation is not due to differences in angular momentum character; indeed, the energy differences for d states are ∼0.8 eV, in the middle of the observed range. However, the LDA-derived vertex function's sensitivity to the local wave function amplitude is highlighted by the nature of orbitals on single atoms, which range from localized to diffuse. We observe that the LDA vertex affects the quasiparticle energies most dramatically for the QP-HOMO corresponding to $d^{10}s \leftarrow d^{10}$ and $d^{10}s^2 \leftarrow d^{10}s$ excitations; the quasiparticle wave functions used in computing these states are overly delocalized due to the use of the LDA exchange−correlation functional. In contrast, the LDA vertex changes the quasiparticle energies the least for the QP-LUMO corresponding to the $d^{10}s \rightarrow d^{10}s^2$ excitation; this wave function is overly localized by the LDA exchange−correlation functional. Despite the increased versatility of the LDA vertex in this context, the inclusion of Γ_{LDA} still does not improve agreement with experiment, and G_0W_0 remains the best predictor of ionization energies for these single atoms. Eigenvalue self-consistency and the LDA vertex correction together also do not exhibit any fortuitous cancellation of effects for this test set.

Finally, in a comparison of GGA and LDA starting points, we observe only minimal differences in the resulting G_0W_0 and ev*GW* energies of s and p states, with energy differences no more than 0.2 eV. However, large differences (0.4−0.8 eV) are observed for the localized d states, bringing both G_0W_0@GGA and ev*GW*@GGA energies closer to experimental measurements. The mean-field GGA electronic structure therefore appears to be a better starting point than the LDA for *GW* calculations, and among the variants of *GW* tested here (using nonhybrid DFT starting points), quasiparticle energies from G_0W_0@GGA provide the best agreement with experimental ionization energies.

4.2. Absorption Energies. *GW*-BSE eigenvalues are computed starting from the variants of *GW* of the previous section and are compared to spin−orbit-averaged experimental absorption energies and TDDFT eigenvalues. We focus on low-lying, spin-conserving excitations promoting electrons from the HOMO to the unoccupied valence s or p shells. Due to the similarity of s and p quasiparticles from *GW* with the LDA and GGA starting points, BSE@G_0W_0@GGA and BSE@ev*GW*@GGA results are computed only for excitations from d states.

In Figure 8, we summarize the error relative to experiment for BSE eigenvalues computed from quasiparticles in the diagonal approximation (eq 24) and BSE eigenvalues computed from quasiparticles that account for off-diagonal terms of the *GW* self-energy (eq 27). Rectangles indicate the ranges from minimum to maximum error across the Cu, Ag, Zn, and Cd test set. In the diagonal approximation, perturbative *GW*-BSE eigenvalues are seen to underestimate absorption energies, with improvements in accuracy for self-consistent *GW*-BSE, which agrees with other recent *GW*-BSE benchmarks of confined systems.[14,70,73] The inclusion of the LDA vertex increases the predicted energies of optical excitations; however, without self-consistency (BSE@$G_0W_0\Gamma_{LDA}$@LDA), this still underestimates excitation energies.

With the inclusion of off-diagonal terms, the predicted absorption energies increase for all variants of *GW*-BSE. This effect occurs because the low-lying LDA (and GGA) unoccupied orbitals are too localized and off-diagonal terms result in improved, more delocalized quasiparticles.[34] With this energy increase, eigenvalue self-consistency no longer improves accuracy for all calculations. BSE@ev*GW*@LDA deteriorates in accuracy compared to BSE@G_0W_0@LDA, but BSE@ev*GW*@GGA is the most accurate variant of conventional *GW* tested,

Table 2. Mean Error (eV) of *GW* Quasiparticle Energies Relative to Experiment, Averaged across the Cu, Ag, Zn, and Cd Test Set, With the Reference Valence Electron Configurations in Bold

	G_0W_0	ev*GW*	$G_0W_0\Gamma_{LDA}$	ev*GW*Γ_{LDA}	G_0W_0	ev*GW*
	@LDA				@GGA	
$\mathbf{d^{10}s^2} \leftarrow d^{10}s$	−0.19	−0.26	0.80	0.69	−0.28	−0.32
$\mathbf{d^{10}s} \rightarrow d^{10}s^2$	−0.23	0.30	0.34	0.96	−0.24	0.26
$\mathbf{d^{10}s} \leftarrow d^{10}$	−0.64	−0.67	0.36	0.31	−0.61	−0.67
$\mathbf{d^{10}} \rightarrow d^{10}s$	−0.32	−0.06	0.52	0.72	−0.36	−0.12
$\mathbf{d^{10}} \leftarrow d^{9}$	−0.59	−1.63	0.22	−0.88	−0.03	−1.06

DOI: 10.1021/acs.jctc.7b00123
J. Chem. Theory Comput. 2017, 13, 2135−2146

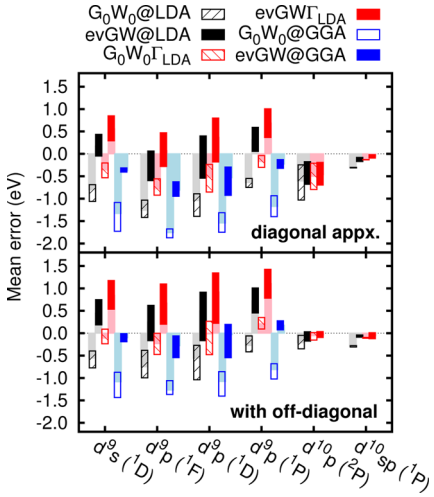

Figure 8. Error of *GW*-BSE predictions relative to experimental absorption energies from a d^{10} (first four sets of bars), $d^{10}s$ (fifth set), or $d^{10}s^2$ (sixth set) electron configuration to the configuration listed along the *x* axis. Rectangles matching the legend indicate the error range across the Cu, Ag, Zn, and Cd test set, with fainter colored bars providing a guide for the eye.

with errors no more than 0.5 eV (see Table 3). Surprisingly, we find that the computationally efficient BSE@$G_0W_0\Gamma_{LDA}$@LDA provides excellent agreement with experiment, comparable to BSE@ev*GW*@GGA. DFT-derived vertex corrections, when combined with the use of the off-diagonal terms of the *GW* self-energy and a consistent level of theory throughout TDDFT, *GW*, and BSE computations, therefore may promote cancellation of effects that allows accurate calculation of BSE energies from inexact *GW* quasiparticles.

5. MONOXIDE ANIONS

We finally compute the binding energies of CuO^-, AgO^-, ZnO^-, and CdO^- from first-principles, limiting our computations here to G_0W_0@LDA and G_0W_0@GGA (Tables 4 and 5).

Neglecting spin−orbit coupling for excitations from the ground states ($X^1\Sigma^+$) of CuO^- and AgO^-, there are two peaks in the experimental anion photoelectron spectra under 3 eV corresponding to photodetachment of an electron and formation of the neutral molecule in the $X^2\Pi$ ground or the $A^2\Sigma^+$ excited state. The difference between G_0W_0 results and the experimental spectra is large, with differences up to 0.9 eV for G_0W_0@LDA and up to 0.7 eV for G_0W_0@GGA. While a small part of this difference may be attributed to our comparison of vertical binding energy predictions (from G_0W_0) to experimental adiabatic binding energies, the bond length changes are small—less than 0.06 Å for CuO^- and less 0.07 Å for AgO^- from Franck−Condon simulations;[23,24] therefore, we believe that the true adiabatic and vertical energies do not differ significantly. The larger error is attributed to the partial d character of the orbital, and we see from CuO^- and AgO^- that even orbitals with only some admixture of d can be difficult to accurately simulate from *GW* calculations.

Errors are smaller in the benchmarks of ZnO^- (up to 0.4 eV for G_0W_0@LDA and up to 0.3 eV for G_0W_0@GGA), which is comparable to the errors of s and p excitations for single atoms at the same levels of theory. These smaller errors, compared to the CuO^- and AgO^- results, are likely due to the minimal d character of the states being studied. The error associated with comparing vertical and adiabatic energies is again expected to be small, with the Franck−Condon simulations predicting bond length changes less than 0.08 Å.[25] Still, we are unable to determine the neutral CdO ground state from these calculations because the $^1\Sigma^+$, $^3\Pi$, and $^1\Pi$ configurations all lie within 0.5 eV of each other. Additional research into improving the numerical and theoretical accuracy of *GW* is needed to allow us to predict these and other properties of transition-metal systems in the future.

Table 4. Vertical Binding Energies (eV) for Excitations from the $X^1\Sigma^+$ Ground States of the CuO^- and AgO^- Anions to the Listed Neutral CuO and AgO Configurations, Compared to Adiabatic Binding Energies from Anion Photoelectron Spectroscopy[23,24]

	CuO^-			AgO^-		
	expt	G_0W_0@LDA	G_0W_0@GGA	expt	G_0W_0@LDA	G_0W_0@GGA
$X^2\Pi$	1.78	2.45	2.05	1.67	2.15	1.81
$A^2\Sigma^+$	2.75	3.37	3.25	2.70	3.56	3.43

Table 5. Vertical Binding Energies (eV) for Excitations from the $X^2\Sigma^+$ Ground States of the ZnO^- and CdO^- Anions to the Listed Neutral ZnO and CdO Configurations, Compared to Adiabatic Binding Energies from Anion Photoelectron Spectroscopy[25]

	ZnO^-			CdO^-	
	expt	G_0W_0@LDA	G_0W_0@GGA	G_0W_0@LDA	G_0W_0@GGA
$X^1\Sigma^+$	2.09	2.31	2.20	2.45	2.36
$a^3\Pi$	2.40	2.38	2.11	2.08	1.81
$A^1\Pi$	2.71	2.68	2.37	2.49	2.15
$b^3\Sigma^+$	3.89	4.32	4.21	4.22	4.17
$B^1\Sigma^+$		5.11	4.99	5.11	4.97

Table 3. Mean Error of *GW*-BSE Eigenvalues (including off-diagonal terms) Associated with Excitations from the QP-HOMO to the Lowest Empty s or p Quasiparticle, Relative to Experimental Energies

transition	TDDFT	BSE@				BSE@	
		G_0W_0	ev*GW*	$G_0W_0\Gamma_{LDA}$	ev*GW*Γ_{LDA}	G_0W_0	ev*GW*
	@LDA	@LDA				@GGA	
$d^{10}s^2 \rightarrow d^{10}sp\ (^1P)$	−0.03	−0.29	−0.07	−0.10	−0.06		
$d^{10}s \rightarrow d^{10}p\ (^2P)$	0.51	−0.21	−0.09	−0.05	−0.04		
$d^{10} \rightarrow d^9p\ (^1P)$	−1.48	−0.28	0.72	0.21	1.11	−0.81	0.18
$d^{10} \rightarrow d^9p\ (^1D)$	−1.90	−0.56	0.50	−0.01	0.92	−1.08	−0.03
$d^{10} \rightarrow d^9p\ (^1F)$	−1.95	−0.75	0.25	−0.23	0.67	−1.27	−0.28
$d^{10} \rightarrow d^9s\ (^1D)$	−1.54	−0.56	0.44	−0.11	0.84	−1.08	−0.10

DOI: 10.1021/acs.jctc.7b00123
J. Chem. Theory Comput. 2017, 13, 2135−2146

6. CONCLUSIONS

In this work, we examine the numerical and theoretical contributions to the accuracy of the *GW* approximation and the BSE equation, applied to Groups IB and IIB atoms and monoxide molecules, and highlight the difficulties in describing excitations involving d orbitals. We illustrate the large *GW* correlation self-energy associated with d states and demonstrate that the complete basis set limit should be used for numerically accurate *GW* quasiparticle energies. We also show that d quasiparticle energies converge more slowly with basis set size than s and p quasiparticles, regardless of the type of basis set used, or if an additional static remainder is applied. We find that energy differences between G_0W_0 and ev*GW* converge more quickly with basis set size than the energy itself, so that ev*GW* energies can therefore be obtained from a smaller basis set if the complete basis set limit of the G_0W_0 energy is already known. For the BSE, we see that using a consistent basis set throughout speeds the convergence of energies with basis set size. For our *GW* and *GW*-BSE calculations, we therefore estimate that excitations involving s and p orbitals are computed with accuracies better than 0.1 eV, while inaccuracies associated with the basis set are ∼0.2 eV for d states.

The other significant numerical approximation, via the use of pseudopotentials, has negligible effect on s and p states. The d state error also appears to be small (less than the extrapolation error) as long as semicore orbitals are not pseudized into the core. On the other hand, our calculations show that relativistic effects can affect self-energies up to a few hundred meV and must be included in benchmark comparisons to experiment. We also demonstrate that exact exchange in the initial mean-field electronic structure can tune G_0W_0 and ev*GW* energy by ∼1 eV. These results support the use of optimal hybrid functional starting points for improved accuracy in *GW* calculations. Starting points using semilocal and local functionals, as in the remainder of this work, generally produce lower quasiparticle energies (higher predicted ionization energies) than hybrid functional and Hartree−Fock electronic structures.

Our benchmarks indicate that eigenvalue self-consistency and the LDA vertex do not improve the ability of the *GW* approximation to predict ionization energies. However, we observe a more varied effect of the approximation vertex function, Γ_{LDA}, than in the past. Instead of resulting in a rigid shift of all quasiparticle energies, the energy changes due to the vertex correction are seen to be related to the localization of the wave functions. We also see that *GW*@GGA energies are very similar to those of *GW*@LDA for s and p states, but for d states and overall, accounting for gradient effects in G_0W_0@GGA calculations produces quasiparticle energies that are slightly more accurate than those in any variants of *GW* that use a LDA starting point.

For two-particle excitations, we are able to obtain excellent agreement between BSE@$G_0W_0\Gamma_{LDA}$@LDA eigenvalues and experimental measurements of absorption, as long as off-diagonal terms are included in the self-energy contributions. The more computationally expensive BSE@ev*GW*@GGA has comparable high accuracy. We observe that cancellation of errors occurs for the *GW* quasiparticles, with the *GW*-BSE variants producing mean errors of ∼0.2 eV. These results suggest that inclusion of off-diagonal elements and further development of vertex corrections may be another route to cheaper, yet more accurate, *GW*-BSE computations of optical properties.

Our benchmarks of transition-metal monoxide anions exhibit differences between G_0W_0 and experimental binding energies that are consistent with benchmarks of the Groups IB and IIB single atoms and ions (a few hundred meV), with larger deviations for quasiparticles with more d character. Multiple states can coexist in such energy ranges, and the uncertainty prevents a definitive prediction of excited-state energy ordering from the *GW* approximation for CdO^-. Therefore, while we are able to limit numerical errors to ∼0.2 eV, scientific questions continue to motivate the search for more advanced techniques in *GW* theory and computation for transition-metal systems.

■ ASSOCIATED CONTENT

Supporting Information

The Supporting Information is available free of charge on the ACS Publications website at DOI: 10.1021/acs.jctc.7b00123.

Additional computational parameters and tabulated *GW*, *GW*-BSE, TDDFT, and experimental reference energies (PDF)

■ AUTHOR INFORMATION

Corresponding Authors

*E-mail: linda.hung@nist.gov (L.H.).
*E-mail: fabien.bruneval@cea.fr (F.B.).
*E-mail: ogut@uic.edu (S.Ö.).

ORCID

Linda Hung: 0000-0002-1578-6152

Funding

L.H., K.B., and S.Ö. would like to thank the U.S. Department of Energy Grant No. DE-FG02-09ER16072, as well as the National Energy Research Scientific Computing Center, a DOE Office of Science User Facility supported by the Office of Science of the U.S. Department of Energy under Contract No. DE-AC02-05CH11231, for computational resources. F.B. acknowledges HPC resources from GENCI-CCRT-TGCC (Grant No. 2016-096018).

Notes

The authors declare no competing financial interest.

■ REFERENCES

(1) Becke, A. D. *J. Chem. Phys.* **1993**, *98*, 1372−1377.
(2) Adamo, C.; Barone, V. *J. Chem. Phys.* **1999**, *110*, 6158−6170.
(3) Heyd, J.; Scuseria, G. E.; Ernzerhof, M. *J. Chem. Phys.* **2003**, *118*, 8207−8215.
(4) Laurent, A. D.; Jacquemin, D. *Int. J. Quantum Chem.* **2013**, *113*, 2019−2039.
(5) Anisimov, V. I.; Zaanen, J.; Andersen, O. K. *Phys. Rev. B: Condens. Matter Mater. Phys.* **1991**, *44*, 943−954.
(6) Anisimov, V. I.; Aryasetiawan, F.; Lichtenstein, A. I. *J. Phys.: Condens. Matter* **1997**, *9*, 767.
(7) Himmetoglu, B.; Floris, A.; de Gironcoli, S.; Cococcioni, M. *Int. J. Quantum Chem.* **2014**, *114*, 14−49.
(8) Hedin, L. *Phys. Rev.* **1965**, *139*, A796−A823.
(9) Aryasetiawan, F.; Gunnarsson, O. *Rep. Prog. Phys.* **1998**, *61*, 237−312.
(10) Strinati, G. *Riv. Nuovo Cimento* **1988**, *11*, 1−86.
(11) Onida, G.; Reining, L.; Rubio, A. *Rev. Mod. Phys.* **2002**, *74*, 601.
(12) Samsonidze, G.; Park, C.-H.; Kozinsky, B. *J. Phys.: Condens. Matter* **2014**, *26*, 475501.
(13) Shirley, E. L.; Martin, R. M. *Phys. Rev. B: Condens. Matter Mater. Phys.* **1993**, *47*, 15404−15412.
(14) Körbel, S.; Boulanger, P.; Duchemin, I.; Blase, X.; Marques, M. A. L.; Botti, S. *J. Chem. Theory Comput.* **2014**, *10*, 3934−3943.

DOI: 10.1021/acs.jctc.7b00123
J. Chem. Theory Comput. 2017, 13, 2135−2146

(15) Kang, Y.; Kang, G.; Nahm, H.-H.; Cho, S.-H.; Park, Y. S.; Han, S. *Phys. Rev. B: Condens. Matter Mater. Phys.* **2014**, *89*, 165130.
(16) Das, S.; Coulter, J. E.; Manousakis, E. *Phys. Rev. B: Condens. Matter Mater. Phys.* **2015**, *91*, 115105.
(17) Scherpelz, P.; Govoni, M.; Hamada, I.; Galli, G. *J. Chem. Theory Comput.* **2016**, *12*, 3523−3544.
(18) Kramida, A.; Ralchenko, Y.; Reader, J.; NIST ASD Team, NIST Atomic Spectra Database (version 5.3). http://physics.NIST.gov/asd (2016).
(19) Lischner, J.; Deslippe, J.; Jain, M.; Louie, S. G. *Phys. Rev. Lett.* **2012**, *109*, 036406.
(20) Perdew, J. P.; Wang, Y. *Phys. Rev. B: Condens. Matter Mater. Phys.* **1992**, *45*, 13244−13249.
(21) Perdew, J. P.; Burke, K.; Ernzerhof, M. *Phys. Rev. Lett.* **1996**, *77*, 3865−3868.
(22) Del Sole, R.; Reining, L.; Godby, R. W. *Phys. Rev. B: Condens. Matter Mater. Phys.* **1994**, *49*, 8024−8028.
(23) Polak, M. L.; Gilles, M. K.; Ho, J.; Lineberger, W. C. *J. Phys. Chem.* **1991**, *95*, 3460−3463.
(24) Andrews, D. H.; Gianola, A. J.; Lineberger, W. C. *J. Chem. Phys.* **2002**, *117*, 4074−4076.
(25) Moravec, V. D.; Klopcic, S. A.; Chatterjee, B.; Jarrold, C. C. *Chem. Phys. Lett.* **2001**, *341*, 313−318.
(26) Tiago, M. L.; Chelikowsky, J. R. *Phys. Rev. B: Condens. Matter Mater. Phys.* **2006**, *73*, 205334.
(27) Hybertsen, M. S.; Louie, S. G. *Phys. Rev. B: Condens. Matter Mater. Phys.* **1986**, *34*, 5390−5413.
(28) Romaniello, P.; Guyot, S.; Reining, L. *J. Chem. Phys.* **2009**, *131*, 154111.
(29) Grüneis, A.; Kresse, G.; Hinuma, Y.; Oba, F. *Phys. Rev. Lett.* **2014**, *112*, 096401.
(30) Hung, L.; da Jornada, F. H.; Souto-Casares, J.; Chelikowsky, J. R.; Louie, S. G.; Öğüt, S. *Phys. Rev. B: Condens. Matter Mater. Phys.* **2016**, *94*, 085125.
(31) Bruneval, F.; Rangel, T.; Hamed, S. M.; Shao, M.; Yang, C.; Neaton, J. B. *Comput. Phys. Commun.* **2016**, *208*, 149−161.
(32) Casida, M. E. *J. Mol. Struct.: THEOCHEM* **2009**, *914*, 3−18.
(33) Kronik, L.; Makmal, A.; Tiago, M. L.; Alemany, M. M. G.; Jain, M.; Huang, X.; Saad, Y.; Chelikowsky, J. R. *Phys. Status Solidi B* **2006**, *243*, 1063.
(34) Rohlfing, M.; Louie, S. G. *Phys. Rev. B: Condens. Matter Mater. Phys.* **2000**, *62*, 4927−4944.
(35) Kaplan, F.; Weigend, F.; Evers, F.; van Setten, M. J. *J. Chem. Theory Comput.* **2015**, *11*, 5152−5160.
(36) van Schilfgaarde, M.; Kotani, T.; Faleev, S. *Phys. Rev. Lett.* **2006**, *96*, 226402.
(37) Hung, L.; Baishya, K.; Öğüt, S. *Phys. Rev. B: Condens. Matter Mater. Phys.* **2014**, *90*, 165424.
(38) Umari, P.; Stenuit, G.; Baroni, S. *Phys. Rev. B: Condens. Matter Mater. Phys.* **2009**, *79*, 201104.
(39) Kang, W.; Hybertsen, M. S. *Phys. Rev. B: Condens. Matter Mater. Phys.* **2010**, *82*, 085203.
(40) Schindlmayr, A. *Phys. Rev. B: Condens. Matter Mater. Phys.* **2013**, *87*, 075104.
(41) Sharifzadeh, S.; Tamblyn, I.; Doak, P.; Darancet, P. T.; Neaton, J. B. *Eur. Phys. J. B* **2012**, *85*, 1−5.
(42) Klimeš, J.; Kaltak, M.; Kresse, G. *Phys. Rev. B: Condens. Matter Mater. Phys.* **2014**, *90*, 075125.
(43) Gulans, A. *J. Chem. Phys.* **2014**, *141*, 164127.
(44) Bruneval, F.; Gonze, X. *Phys. Rev. B: Condens. Matter Mater. Phys.* **2008**, *78*, 085125.
(45) Berger, J. A.; Reining, L.; Sottile, F. *Phys. Rev. B: Condens. Matter Mater. Phys.* **2010**, *82*, 041103.
(46) Berger, J. A.; Reining, L.; Sottile, F. *Phys. Rev. B: Condens. Matter Mater. Phys.* **2012**, *85*, 085126.
(47) Steinbeck, L.; Rubio, A.; Reining, L.; Torrent, M.; White, I. D.; Godby, R. W. *Comput. Phys. Commun.* **2000**, *125*, 105−118.
(48) Friedrich, C.; Schindlmayr, A.; Blügel, S.; Kotani, T. *Phys. Rev. B: Condens. Matter Mater. Phys.* **2006**, *74*, 045104.
(49) Samsonidze, G.; Jain, M.; Deslippe, J.; Cohen, M. L.; Louie, S. G. *Phys. Rev. Lett.* **2011**, *107*, 186404.
(50) Jiang, H.; Blaha, P. *Phys. Rev. B: Condens. Matter Mater. Phys.* **2016**, *93*, 115203.
(51) Kang, W.; Hybertsen, M. S. *Phys. Rev. B: Condens. Matter Mater. Phys.* **2010**, *82*, 195108.
(52) Deslippe, J.; Samsonidze, G.; Jain, M.; Cohen, M. L.; Louie, S. G. *Phys. Rev. B: Condens. Matter Mater. Phys.* **2013**, *87*, 165124.
(53) Gao, W.; Xia, W.; Gao, X.; Zhang, P. *Sci. Rep.* **2016**, *6*, 36849.
(54) Halkier, A.; Helgaker, T.; Jørgensen, P.; Klopper, W.; Koch, H.; Olsen, J.; Wilson, A. K. *Chem. Phys. Lett.* **1998**, *286*, 243−252.
(55) Bruneval, F. *J. Chem. Phys.* **2012**, *136*, 194107.
(56) Kaplan, F.; Harding, M. E.; Seiler, C.; Weigend, F.; Evers, F.; van Setten, M. J. *J. Chem. Theory Comput.* **2016**, *12*, 2528−2541.
(57) Truhlar, D. G. *Chem. Phys. Lett.* **1998**, *294*, 45−48.
(58) Reis, C. L.; Pacheco, J. M.; Martins, J. L. *Phys. Rev. B: Condens. Matter Mater. Phys.* **2003**, *68*, 155111.
(59) Oliveira, M. J. T.; Nogueira, F. *Comput. Phys. Commun.* **2008**, *178*, 524−534.
(60) Troullier, N.; Martins, J. L. *Phys. Rev. B: Condens. Matter Mater. Phys.* **1991**, *43*, 1993−2006.
(61) Rohlfing, M.; Krüger, P.; Pollmann, J. *Phys. Rev. Lett.* **1995**, *75*, 3489−3492.
(62) Marini, A.; Onida, G.; Del Sole, R. *Phys. Rev. Lett.* **2001**, *88*, 016403.
(63) Tiago, M. L.; Ismail-Beigi, S.; Louie, S. G. *Phys. Rev. B: Condens. Matter Mater. Phys.* **2004**, *69*, 125212.
(64) Fleszar, A.; Hanke, W. *Phys. Rev. B: Condens. Matter Mater. Phys.* **2005**, *71*, 045207.
(65) Umari, P.; Fabris, S. *J. Chem. Phys.* **2012**, *136*, 174310.
(66) Li, X.-Z.; Gómez-Abal, R.; Jiang, H.; Ambrosch-Draxl, C.; Scheffler, M. *New J. Phys.* **2012**, *14*, 023006.
(67) Kotani, T.; van Schilfgaarde, M. *Solid State Commun.* **2002**, *121*, 461−465.
(68) van Schilfgaarde, M.; Kotani, T.; Faleev, S. V. *Phys. Rev. B: Condens. Matter Mater. Phys.* **2006**, *74*, 245125.
(69) Gómez-Abal, R.; Li, X.; Scheffler, M.; Ambrosch-Draxl, C. *Phys. Rev. Lett.* **2008**, *101*, 106404.
(70) Blase, X.; Boulanger, P.; Bruneval, F.; Fernandez-Serra, M.; Duchemin, I. *J. Chem. Phys.* **2016**, *144*, 034109.
(71) Baym, G. *Phys. Rev.* **1962**, *127*, 1391−1401.
(72) Blase, X.; Attaccalite, C.; Olevano, V. *Phys. Rev. B: Condens. Matter Mater. Phys.* **2011**, *83*, 115103.
(73) Jacquemin, D.; Duchemin, I.; Blase, X. *J. Chem. Theory Comput.* **2015**, *11*, 3290−3304.
(74) Marom, N.; Caruso, F.; Ren, X.; Hofmann, O. T.; Körzdörfer, T.; Chelikowsky, J. R.; Rubio, A.; Scheffler, M.; Rinke, P. *Phys. Rev. B: Condens. Matter Mater. Phys.* **2012**, *86*, 245127.
(75) Morris, A. J.; Stankovski, M.; Delaney, K. T.; Rinke, P.; García-González, P.; Godby, R. W. *Phys. Rev. B: Condens. Matter Mater. Phys.* **2007**, *76*, 155106.

DOI: 10.1021/acs.jctc.7b00123
J. Chem. Theory Comput. 2017, 13, 2135−2146